Inorganic Chemistry
Cite This: Inorg. Chem. 2019, 58, 10912−10919
Article
pubs.acs.org/IC

Two-Dimensional Metal−Organic Framework Nanosheets as a Dual Ratiometric and Turn-off Luminescent Probe

Rawan Al Natour,[†] Zeinab Kara Ali,[†] Abdeljalil Assoud,[‡] and Mohamad Hmadeh*[,†]

[†]Chemistry Department, American University of Beirut, P.O. Box 11-0236, Riad El-Solh, Beirut 1107 2020, Lebanon
[‡]Department of Chemistry, University of Waterloo, Waterloo N2L 3G1, Ontario, Canada

Supporting Information

ABSTRACT: Current research on metal−organic framework (MOF) luminescent sensing probes focuses on the design of three-dimensional bulk-sized MOFs that in return limits their up-close interactions with targeted guest molecules. In this work, we report a two-dimensional (2D) copper-based metal−organic framework, namely, AUBM-6, synthesized via solvothermal method from isonicotinic acid linker and copper(II) ion. The resulting 2D-layered MOF crystals were highly fluorescent in their exfoliated form and, therefore, explored for detecting several solvents, where a ratiometric selectivity was shown toward acetone. Metal ion sensing was also performed, by which fluorescent detection was observed to have the highest turn-off quenching efficiency toward Pd^{2+}.

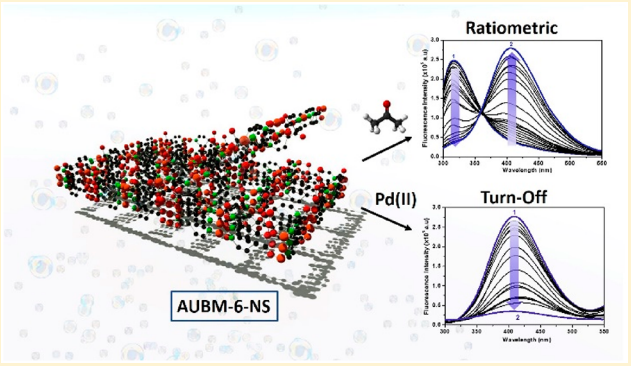

INTRODUCTION

Metal−organic frameworks, known as MOFs, are porous materials that are self-assembled from metal ions/cluster and multitopic organic linkers.[1−3] The synthesis of MOFs with various pore sizes has attracted broad interest, due to the promising applications of MOFs in gas storage/separation, sensing, molecular sieving, and catalysis.[4−6] Among their various applications, the development of sensitive and selective luminescent diagnostics toward late and heavy transition metals is of immense interest, due to their various cytotoxic effects and environmental and health complexities.[7] On one hand, a rare transition metal, palladium (Pd^{2+}), is known to have a wide spectrum of hazardous health effects even in minimal concentrations, which include skin and eye allergies, perturbations of cellular processes, and various environmental hazards.[7−9] For instance, previous investigations have indicated that Pd^{2+} ions can bind to DNA, proteins, or other macromolecules such as vitamin B6.[10] Apart from this, it is well-established that several environmental agencies restrict the maximum dietary intake of palladium to less than 1.5−15 μg per day per person; in addition, its threshold in drugs is 5−10 ppm.[11,12]

On the other hand, acetone, being a common solvent that plays a vital role in the chemical industry, is known to be volatile, by which it irritates the eyes, skin, and respiratory tract upon too much exposure.[13] Recently, luminescent MOFs have attracted remarkable attention due to their advantageous ability to entrap guest molecules of interest within their pores and keep them in close proximity to their active centers.[14] Currently, there exist several MOFs previously reported for acetone sensing;[13,15−18] however, most of these MOFs exhibit lanthanide-based metal centers, and only a few transition-metal centers demonstrate unique selectivity toward detection of acetone molecule. It is worthy to note that most of the latter-reported MOFs exhibit a turn-off luminescent sensor; none of which exhibit a ratiometric characteristic probe. Until recently, ratiometric detection has taken a high toll in being successful methods in addressing hybrid systems or organic fluorophores.[19]

Current research on MOF luminescent sensing probes focus on the design of three-dimensional (3D) bulk-sized MOFs that in return limits their up-close interactions with targeted metal ions.[15,20−22] To synthesize an effective MOF sensor, binding sites, powerful luminophore, and a stable morphology are needed.[23] Hence, the pore sizes and topologies of MOFs, in addition to the presence of different exposed functional sites such as $-NH_2$, −OH, and pyridine sites, act to enhance the MOF's ability to recognize different metal ions.[23−25] Adding to that, using π-conjugated organic molecules also play a significant role in providing adequate binding sites for different metal ions.[26−28] For instance, isonicotinic acid (INA) ligand (Scheme 1), having a whole π-conjugated backbone, tends to afford $\pi-\pi$ interactions either between adjacent conjugated ligands or adjacent guest molecules.

It is still a great challenge to obtain two-dimensional (2D) MOFs with atomic or molecular thickness in high yields; nevertheless, previous methods have reported the exfoliation of 3D layered MOFs into their complementary 2D nanosheets, hence retaining their structure and topology.[25,29−32] Such

Received: May 7, 2019
Published: July 30, 2019

DOI: 10.1021/acs.inorgchem.9b01315
Inorg. Chem. 2019, 58, 10912−10919

Scheme 1. Synthesis Route of AUBM-6 Crystals Starting from INA Ligand

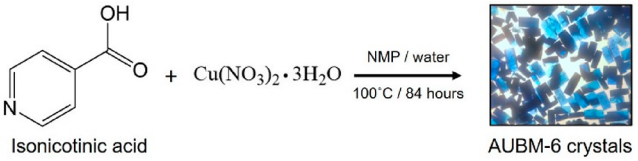

exfoliation process is mainly based on delaminating these frameworks that are held together by weak interactions including van der Waals or hydrogen bonding.[29,32] Moreover, having relatively increased surface areas and ultrathin thickness, the exfoliated 2D nanosheets exhibit more accessible active sites.[33] As a result, the complementary luminescent sensing properties either increase in sensitivity, rate, activity, or efficiency.

Herein, we report the synthesis and characterization of a chemically stable (in common solvents) 2D-layered MOF, namely, AUBM-6 (AUBM = American University of Beirut Materials) and the fabrication of its layered structure into its complementary 2D thin nanosheets via top-down liquid ultrasonication exfoliation method. While the copper-based MOF was investigated for photoluminescence (PL) sensing toward different metal ions and solvents, it was concluded that AUBM-6 is selective toward Pd^{2+} and acetone specifically having turn-off and ratiometric diagnostic probes, respectively. To the best of our knowledge, there is not a reported transition-metal-based MOF exhibiting a ratiometric mechanism toward acetone detection.

EXPERIMENTAL SECTION

Materials and Methods. All reagents and chemicals were commercially available from Sigma-Aldrich and used without any further purification. The infrared (IR) spectra were recorded on a Fourier transform infrared (FT-IR) spectrometer Thermo-Nicolet working in the transmittance mode, in the 450−3950 cm^{-1} range. Thermogravimetric analysis (TGA) was performed with Netzsch TG 209 F1 Libra apparatus. Single-crystal X-ray data were collected using Bruker Kappa APEX II diffractometer with Mo Kα (λ = 0.710 73 Å); the data were corrected for Lorentz and polarization, and a multiscan absorption correction was applied using the APEX III suite. The structure was solved using the direct method and refined using least-square method incorporated in SHELXTL package. Since the crystals were twinned due to the stacking of the plates, one phenyl ring was partially disordered, while the solvent molecules were completely disordered. Powder X-ray diffraction (PXRD) patterns were collected using a Bruker D8 advance X-ray diffractometer (Bruker AXS GmbH) at 40 kV, 40 mA (1600 W) using Cu Kα radiation (λ = 1.5418 Å). Scanning electron microscopy (SEM) was performed using an MIRA3 Tescan electron microscope, where the samples were first coated with a thin layer of gold. The Brunauer−Emmett−Teller (BET) surface area was measured using a Quantachrome-NOVA 2200e-Surface Area and Pore Size Analyzer. The absorption spectra were recorded at room temperature using JASCOV-570 UV−vis−NIR (NIR = near-infrared) spectrophotometer. The steady-state fluorescence measurements were recorded with resolution increment of 1 nm, slit 5, using a HORIBA Jobin Yvon Fluorolog-3. The excitation source was 100 W xenon lamp, and the detector used was an R-928 operating at a voltage of 950 V. To regulate the temperature, a thermostat was coupled with the sample holder.

Synthesis of AUBM-6. $Cu(NO_3)_2{\cdot}3H_2O$ (0.4095 mmol, 98.94 mg) and INA (0.0819 mmol, 10 mg) were dissolved in a mixture of 2 mL of *N*-methyl-2-pyrrolidone (NMP) and 1 mL of deionized water in a 4 mL vial. After it was sonicated for 10 min, the subsequent solution was heated at 100 °C for 84 h. The resulting blue single crystals (Scheme 1) were left to cool at room temperature, then washed three times with NMP and three times with methanol to obtain 83% yield based on INA. The fabrication of AUBM-6 nanosheets (AUBM-6-NS) was done via top-down liquid ultrasonication exfoliation method, by which 10 mg of the crystals were placed in 10 mL of acetonitrile and ultrasonicated for 10 h at room temperature. A blue colloidal suspension was obtained and centrifuged at 10 000 rpm for 1 h to get the AUBM-6-NS materials.

Solvent Titrations. Suspensions of AUBM-6-NS were initially prepared by dispersing 5.00 mg in 10 mL of acetonitrile (CH_3CN) solution for 10 min. Microvolumes (10 to 1000 μL) of 2% by volume of acetone, chloroform, dichloromethane, dimethylformamide (DMF), dimethylacetamide (DMA), tetrahydrofuran (THF), *N*-methyl-2-pyrrolidone (NMP), methanol, 1-butanol, and 2-propanol in addition to pure deionized water were gradually sensed against 3 mL of standard emulsion of AUBM-6-NS. Intensity enhancement and a bathochromic shift demonstrating a ratiometric probe was only observed for acetone.

Metal Ions Titrations. The nitrate metal salts used for luminescence sensing at room temperature are M^{n+}: [Fe^{3+}, Fe^{2+}, Al^{3+}, As^{3+}, Mg^{2+}, Co^{2+}, Cd^{2+}, Ni^{2+}, Cu^{2+}, Cu^{+}, Mn^{2+}, Hg^{2+}, Zn^{2+}, Cr^{3+}, Ca^{2+}, Pd^{2+}, and Ag^{+}]. AUBM-6 (5.00 mg) and AUBM-6-NS (5.00 mg) were dispersed and ultrasonicated separately in 10 mL of acetone for 10 min, where the colloidal suspension was obtained for each. The sensing measurements of 3 mL of standard emulsions of AUBM-6 and AUBM-6-NS were performed by adding gradual volumes of the metal cation solutions having 2.5 ppm initial concentrations. Each titration measurement was performed twice for reproducibility. No shift in the main absorbance band of the MOF was observed; however, only intensity quenching was noted in the emission spectra during titrations.

RESULTS AND DISCUSSION

Description of Crystal Structure. AUBM-6 blue single crystals are obtained by heating a mixture of INA ligand and Cu(II) in NMP and water at 100 °C for 84 h. The collected crystals are nonsoluble and stable in common organic solvents. AUBM-6 crystals feature a 2D rectangular prism shape with multilayered structure topology, as it can be seen in Figure 1A.

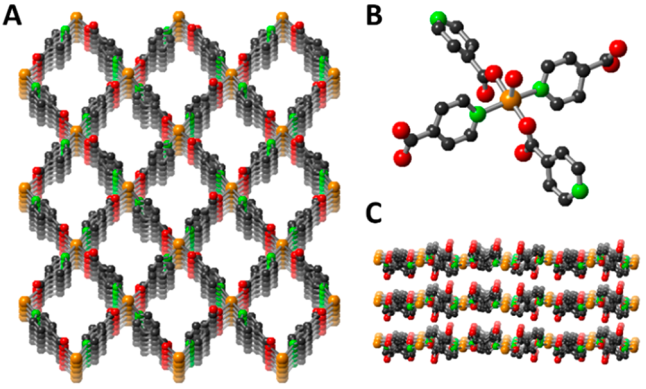

Figure 1. (A) Multilayer view of the 1D channels of AUBM-6 ($C_{17}H_{17}CuN_3O_6$). (B) Coordination environment of the Cu^{2+} ion in AUBM-6. (C) 2D multilayer side view of AUBM-6. Copper (gold); oxygen (red); nitrogen (green), carbon (black).

Single-crystal X-ray diffraction analysis reveals that the compound crystallizes in the orthorhombic, non-centrosymmetric space group $Pca2_1$ with the lattice parameters of a = 23.8349(6) Å, b = 5.80370(10) Å, c = 13.1873(3) Å, and cell volume 1824.21(7) $Å^3$. All the atoms are located at the general Wyckoff position 4a. The asymmetric unit cell contains one Cu(II) ion, two crystallographically independent INA ligands,

DOI: 10.1021/acs.inorgchem.9b01315
Inorg. Chem. 2019, 58, 10912−10919

one water molecule, and one NMP solvent. The obtained formula of the structure is $C_{17}H_{17}CuN_3O_6$. To verify that the geometry of the penta-coordinated Cu(II) in the MOF structure is square pyramidal, the structural parameter ($\tau_5 = \frac{\beta - \alpha}{60}$) is investigated, by which its value was found to be 15.8%, where α (N−Cu−N) = 168.9°and β (O−Cu−O) = 178.5° represent the two basal angles. Hence, in ideal square pyramidal geometry, τ_5 = 0%, α = 180°, and β = 180° are reported.[34,35] The obtained τ_5 demonstrates a very small deviation of 15.8% due to the distortions in INA ligand. The Cu(II) ion is coordinated to four INA ligands bonded through alternating carboxylate and nitrogen ends to form one mononuclear heterotopic secondary building unit (SBU) and also connected to water oxygen with bond distances: Cu−O (carboxylate) ∼1.94 Å, Cu−N 2.02 and 2.04 Å, and Cu−O (water) ∼2.24 Å. The coordination of water oxygen to Cu(II) center orients perpendicularly to the square planar INA ligands, forming the square pyramidal geometry; nevertheless, this oxygen was omitted for structure clarity purposes. The Cu-INA ligands are bridging through the N and O to form 2D multilayers as shown in Figure 1C. The carboxylate and pyridine units attached to Cu(II) are in trans positions; hence, two of the uncoordinated oxygen atoms point either toward or away from the subsequent layer. There exist one-dimensional (1D) porous channels centered around the distorted squared $Cu_4(INA)_4$ units with the Cu−Cu distances of 8.85 and 8.93 Å and the Cu−Cu diagonal distances of 11.93 and 13.19 Å (Figure S1). The distance between these layers is the size of the *b*-axis, and it is ∼5.80 Å taking the Cu ions as reference. The layers are weakly connected to each other through hydrogen bonds between water and nitrogen and carboxylate groups. These interactions present between the layers are critical for delamination to occur by ultrasonic exfoliation.

PXRD Patterns and Thermogravimetric Analysis. The phase purity of the synthesized 2D AUBM-6 and AUBM-6-NS was verified by PXRD by comparing the simulated and experimental patterns. The experimental diffraction peaks are shown to be in good agreement with the simulated one as shown in Figure S2. This verifies the crystalline identity and the purity of AUBM-6 and AUBM-6-NS samples. The thermostability of AUBM-6 was studied by thermogravimetric analysis (TGA) (Figure S3) at the temperature range of 30−700 °C. The TGA curve represented a two-steps weight degradation within this temperature range. The first step is demonstrated from 30 to 100 °C with an estimate of 3.71% weight loss attributed to the escape of water molecules from the framework. The second 53.13% weight loss is represented by a steep declination at 250 °C establishing a correlation with the decomposition of the MOF structure and discharge of the organic ligands.

FT-IR Spectrum Analysis and BET Surface Area Measurement. Analysis of the FT-IR spectrum of AUBM-6 shows two peaks at 1384.6 and 1608.1 cm^{-1} indicating the bending vibrations of N−H and the asymmetric stretching vibrations of the carbonyl group, respectively (Figure S4). These peaks respectively correspond to the downfield shift toward lower wavenumbers from the original peaks of INA present at 1409.7 and 1712.5 cm^{-1} thus to lower energies, which favor the coordination of the metal cations to the organic linkers. The absence of the −OH stretching band at 2429.3 cm^{-1} in AUBM-6 verifies the carboxylate coordination group in INA to Cu^{2+}. The N_2 sorption isotherm of AUBM-6 at 77 K shows a reversibility adsorption behavior characterizing the layered microporous material (Figure S5). BET surface area was calculated to be 233 $m^2 \cdot g^{-1}$.

Effect of Exfoliation on PL-Spectra of AUBM-6. The ultrasonic exfoliation of AUBM-6 resulted in few-layer nanosheets. To further confirm the delamination procedure, SEM was performed to investigate the morphologies of the exfoliated and nonexfoliated crystals (Figure S6). As shown in Figure 2A, SEM images of AUBM-6 reveal bulk rectangular

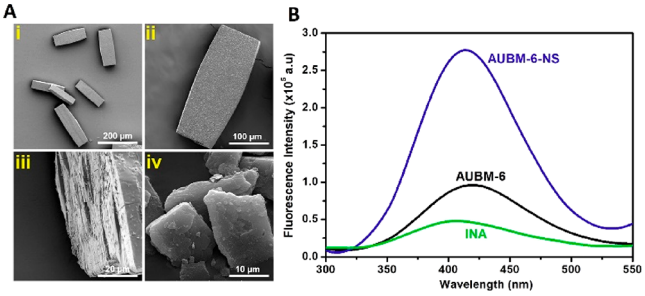

Figure 2. (A) SEM images of (i) bulk crystals of AUBM-6, (ii) single crystal of AUBM-6, (iii) 2D multilayer side view morphology of AUBM-6, and (iv) exfoliated morphology of AUBM-6-NS. (B) PL spectra of INA, AUBM-6, and AUBM-6-NS in acetone at λ_{ex} = 285 nm.

crystals with a multilayered structure having lateral dimensions up to 50 μm. In contrast, SEM images of the exfoliated AUBM-6-NS show a significant decrease in the lateral dimensions that varies to less than 200 nm. This demonstrates that the multilayered structure of AUBM-6 withstands a strongly bonded intralayer assembly and exhibits weakly bonded interlayer interactions, which allow it to be readily delaminated into few-layer nanosheets, hence preserving its initial parent topology as evidenced by the PXRD pattern of the crystals performed after sonication (Figure S2). One reasonable explanation of the retention of topology between the 2D bulk and exfoliated materials is that ultrasonic waves generate shear forces or cavitation bubbles upon the layered species, generating high energies that result from the collapse of bubbles. Thus, such voids lead to break up of the weak bonds between the layered species into their complementary single or multilayered nanosheets without interfering in the intralayer structure of the MOF.[27] The PL properties of the free INA ligand, AUBM-6, and AUBM-6-NS crystals were investigated at room temperature. As shown in Figure S7, there is no overlap between the absorption spectrum of acetone and the excitation band of AUBM-6-NS, which confirms that acetone has no competitive energy absorption within the MOF framework.[19] As a result, this shows that acetone molecules may enhance ligand-to-metal charge transfer efficiency from INA ligand to Cu^{2+} centers. Upon excitation at 285 nm (Figure S8), AUBM-6 shows a broad emission peak at 409 nm, which may be attributed to $\pi-\pi^*$ or $n-\pi^*$ transitions (Figure 2B). Moreover, having the same emission band as INA, AUBM-6 is observed to have an induced ligand centered emission. It is noteworthy that the emission intensity of AUBM-6-NS is shown to be up to threefold greater than that of the bulk AUBM-6. Hence, it is proposed that the PL spectra of the bulk AUBM-6 may exhibit a self-quenching mechanism, upon which their respective delamination into ultrathin nanosheets is observed to activate the MOF into its PL properties.

DOI: 10.1021/acs.inorgchem.9b01315
Inorg. Chem. 2019, 58, 10912−10919

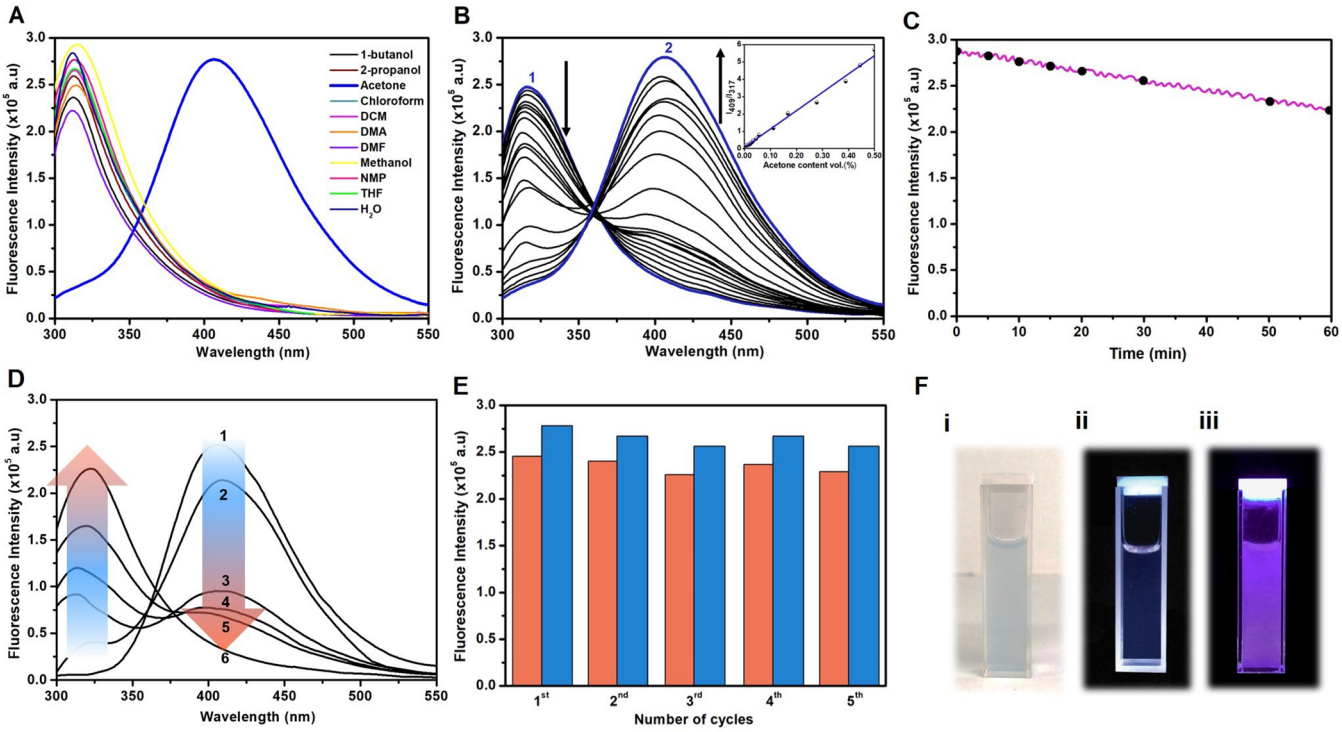

Figure 3. (A) PL spectra of AUBM-6-NS upon addition of different organic solvents (2.0 vol%) at 1000 μL. (B) Ratiometric probe of AUBM-6-NS initially dispersed in CH_3CN upon gradual titration with acetone at (1) 0 and (2) 1000 μL. (inset) Intensity ratio at 409 and 317 nm PL emission of AUBM-6-NS upon addition of different amounts of acetone (at λ_{ex} = 285 nm). (C) Fluorescence intensity vs time trajectories of AUBM-6-NS upon continuous excitation at λ_{ex} = 285 nm. (D) Reversibility of ratiometric peaks upon gradual increase in temperature from (1) 25, (2) 30, (3) 35, (4) 40, (5) 45, and (6) 50 °C at λ_{ex} = 285 nm. (E) Recyclability of the ratiometric peaks of AUBM-6-NS after temperature increase (pink: I_{317}) and (blue: I_{409}). (F) Colorimetric changes of AUBM-6-NS in (i) acetone under visible light, (ii) acetonitrile under ultraviolet light, and (iii) acetone under ultraviolet light.

Table 1. Literature Survey about Previously Reported MOFs towards Acetone Sensing

luminescent materials	detection method	LOD_{min} (vol%)	ref
$Eu(BTC)(H2O)_{2.5}$	turn-off	0.31	17
$Eu(BTB)(H2O)_2$	turn-off	0.010	13
$Tb_4(\mu_6\text{-}L)_2(\mu\text{-}HCOO)(\mu_3\text{-}OH)_3(\mu_3\text{-}O)(DMF)_2(H_2O)_4$	turn-off	0.20	18
$[Cd_3(tib)_2(BTB)_2(DEF)_3]_4(H_2O)_5$	turn-off	0.075	16
$Cd_3(tib)_2(BTB)_2(DMA)_2(H2O)_2$	turn-off	0.085	16
$Yb(BPT)(H_2O)(DMF)_{1.5}(H2O)_{1.25}$	turn-off	0.50	36
$Tb(BTC)(H2O)_6$	turn-off	0.28	37
$[Cd_3(L)(H_2O)_2(DMF)_2](DMF)_5$	turn-off	0.10	38
$Cd_3(dib)(L)](H2O)_3(DMA)_5$	turn-off	0.20	38
AUBM-6-NS	ratiometric	0.0067	this work

Ratiometric Selectivity toward Acetone. AUBM-6-NS crystals were initially dispersed in acetonitrile CH_3CN solution at an excitation wavelength of 285 nm. The PL spectra gave a characteristic emission band at 317 nm as shown in Figure 3A. With gradual titrations of different organic solvents, in addition to deionized water, the resultant peak emissions showed no significant change at 317 nm, except for acetone, where a red shift to 409 nm was observed. The most interesting feature is that, with the addition of increasing volumes of acetone, the luminescent intensity at 317 nm substantially decreased, and a broad new emission peak at 409 nm gradually appeared (Figure 3B). The addition of only 0.0067% of acetone initiates quenching of the initial parent intensity; thus, the addition of 0.5% of acetone can completely quench the band centered at 317 nm (I_{317}) and generate a completely red-shifted peak centered at 409 nm (I_{409}). Such a significant bathochromic shift not only enables the accurate sensing of acetone but also induces an accurate measurement of the two emission intensities generated by a large ratiometric value variation. In fact, as the volume of acetone is increased, the emission intensity ratio (I_{409}/I_{317}) is found to be linearly proportional to the content of acetone added in the range of 0.0067−0.50%. The proposed mechanism behind the observed quenching effect of the parent peak may be attributed to minor interactions between the MOF structure and acetone, by which upon excitation, energy is transferred from the INA ligands to acetone molecules resulting in a significant ratiometric effect. It is also suggested that the acetonitrile molecules that are weakly coordinated to the open metal sites of Cu^{2+} are gradually replaced by the acetone molecules, leading to their significant signal diminishing and peak-shifting effects. Unlike most lanthanide and transition-metal-based

DOI: 10.1021/acs.inorgchem.9b01315
Inorg. Chem. 2019, 58, 10912−10919

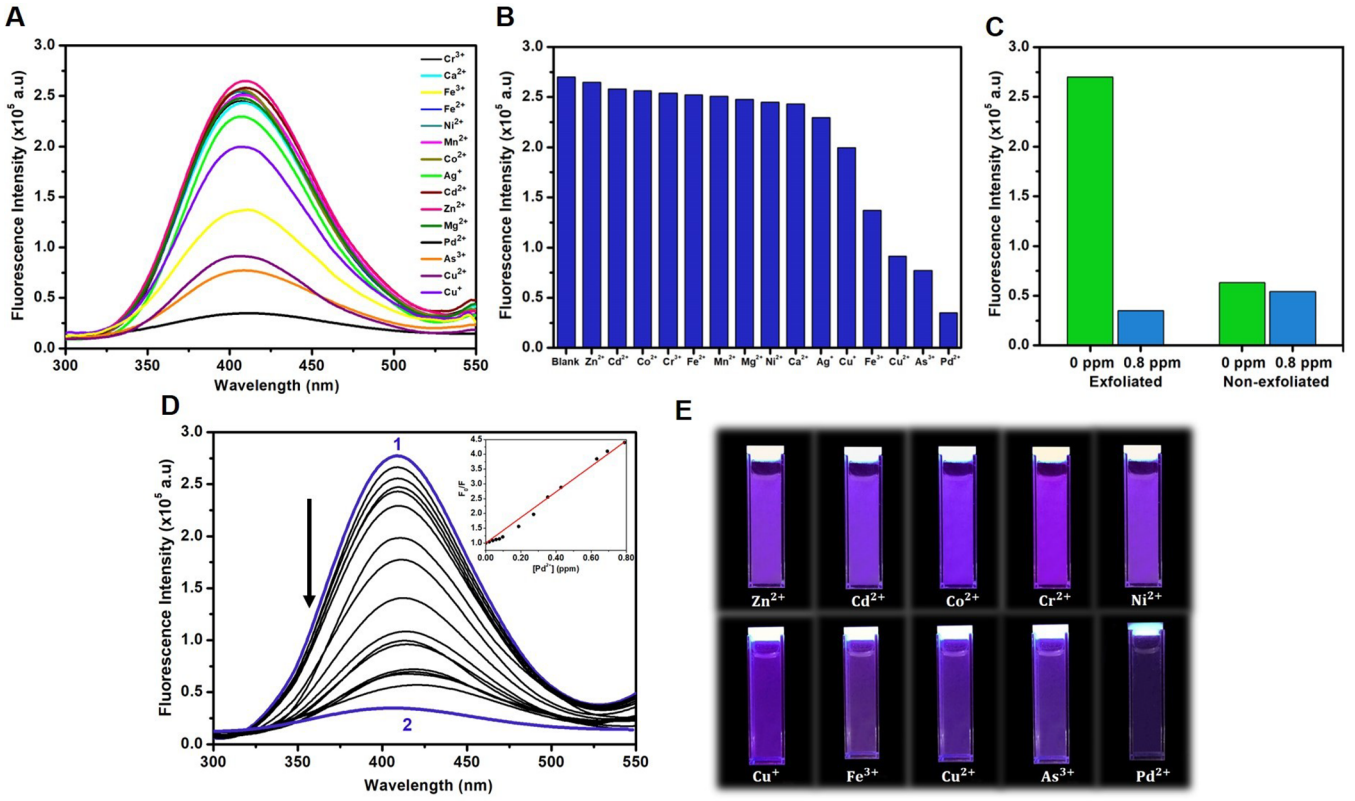

Figure 4. (A, B) PL quenching intensities of different metal cations upon addition of 0.8 ppm at λ_{ex} = 285 nm. (C) Effect of exfoliation on sensing Pd^{2+} at 0.8 ppm of AUBM-6-NS and AUBM-6. (D) PL spectra of AUBM-6 upon gradual titrations at (1) 0 and (2) 0.8 ppm of Pd^{2+} ions at λ_{ex} = 285 nm. (inset) Stern–Volmer plot demonstrating gradual Pd^{2+} titrations. (E) Colorimetric changes of AUBM-6-NS in solution upon addition of 0.8 ppm of different metal cations.

MOFs that require preactivation before performing the PL spectra due to the hindrance effect of other solvent molecules present in their voids, the activation of AUBM-6-NS prior to acetone detection is bypassed due to its ratiometric characteristic probe. Furthermore, as shown in Table 1, it is important to note that previously reported MOFs exhibit a turn-off mechanism toward acetone sensing, unlike AUBM-6-NS, which interestingly demonstrates a ratiometric detection.

The PXRD pattern of AUBM-6-NS after acetone detection (Figure S2) proves to be consistent with original sample, thus ruling out the collapse of the framework. The photostability of AUBM-6-NS in acetone was also examined as shown in Figure 3C. It is noteworthy that, with continuous excitation at 285 nm and collection of emission intensity at 409 nm for 60 min, only a 7% decrease in PL intensity was observed; hence, it is believed that the dispersion of AUBM-6-NS in acetone is concluded to be stable and far from significantly inducing photodegradation. Moreover, the reversibility potential of the newly originated peak at 409 nm upon gradual increase in temperature was examined. Impressively, upon increasing the temperature from 25 to 30 °C, a noticeable decrease in I_{409} and an increase in I_{317} is observed as shown in Figure 3D. With further increase in temperature, a continuous decrease in I_{409} is noticed, until T = 50 °C, where a complete quenching resulted, and a complete regeneration of I_{317} occurred. The gradual evaporation of acetone molecules resulted in the blue shift of intensity to its original parent peak (I_{317}), proving the AUBM-6-NS selectivity toward acetone. Moreover, to check the recyclability of the latter process, acetone was readded, and the effect of temperature increase on the ratiometric process was studied. Remarkably, the regeneration of the peak at 317 nm and disappearance of the peak at 409 nm was achieved up to five times with no significant change in the peak intensities as shown in Figure 3E. Colorimetric changes corresponding to the ratiometric changes were also examined. As it can be seen in Figure 3F, exposing the dispersed AUBM-6-NS in acetonitrile to ultraviolet radiation exhibits no visible emission (I_{317}), in contrast to that of acetone, where a pale violet color is observed (I_{409}).

PL-Spectra of AUBM-6-NS Turn-off toward Pd^{2+}. Considering the open carboxylate sites present on the INA ligand coordinated within the MOF framework, we examined its potential for sensing different metal cations in water. After the dispersion of AUBM-6-NS in acetone, different metal cations having initial concentrations of 2.5 ppm were individually and gradually titrated upon its standard emulsion. As shown in Figure 4A,B, most metals examined either had no or a slight significant effect on the PL intensity, except for Pd^{2+}, by which a substantial quenching, up to 90%, occurred. Initially, the quenching interaction began with the addition of 0.02 ppm of Pd^{2+}, where the gradual increase in its concentration resulted in a decrease in its PL intensity reaching a maximum quenching at 0.8 ppm (Figure 4D). Moreover, the effect of exfoliation on the sensing properties of the MOF was further studied. As shown in Figure 4C, gradual titrations on emulsions of AUBM-6 showed minimal quenching properties in addition to its relatively lower luminescence intensity compared to that of AUBM-6-NS. This proposes that, upon exfoliation, more open binding sites are exposed, which attract more Pd^{2+} ions into the MOF pores

DOI: 10.1021/acs.inorgchem.9b01315
Inorg. Chem. 2019, 58, 10912−10919

and keep them in close proximity to the conjugated ring present in INA linker, hence causing a perturbation within its electronic structure. Such perturbation causes an alteration in the excited state of the INA linker, which in return inhibits ligand-to-metal charge transfer (LMCT), inducing quenching. Colorimetric changes upon titration of different metal cations at 0.8 ppm was also observed (Figure 4E). With the addition of Pd^{2+} ion, the pale violet color disappeared under ultraviolet light illumination, as it can be clearly observed by the naked eye. In contrast, with the addition of other metal analytes, no considerable change in the color of the solution was noticed. To understand the selective quenching behavior of Pd^{2+} toward AUBM-6-NS in the presence of other metal ions, competition experiments were performed as shown in Figures S9−S12. With the addition of different metal ions at increasing concentrations, none or a slight quenching was observed up to a saturation limit, by which following the addition of Pd^{2+}, the PL intensity was completely quenched, hence verifying its remarkable selectivity. Furthermore, the effect of pH on the quenching response of AUBM-6-NS toward Pd^{2+} was studied at pH = 4, 6, and 10 (Figure S13). Results show that, as pH decreases, the quenching efficiency was enhanced, where at pH = 4, a 100% quenching was observed upon addition of 0.57 ppm of Pd^{2+} compared to that of 0.8 ppm at neutral pH. In contrast, as the medium turns basic, quenching efficiency was recorded to decrease. Interestingly, the control experiments demonstrate that the PL of AUBM-6-NS is pH-independent, where no change in intensity was observed upon changing the pH value. However, the observed slight decrease in PL intensity of AUBM-6-NS in the latter pH (Figure S13) is due to dilution effects (upon addition of 700 μL). To explain this enhancement in the quenching behavior, we investigated the distribution curve of Pd^{2+} species in aqueous solution at different pH values.[39] It can be seen that, at high pH values (>8), the hydroxylated species of Pd^{2+} are predominant. Hence, it is concluded that the nonhydroxylated versions had higher affinities toward AUBM-6-NS, which resulted in a complete quenching of the PL intensity at pH = 4 at lower concentrations. This shows that Pd^{2+} ion detection is not only sensitive in neutral mediums but also in acidic environments as well. Analysis of the steady-state emission data using the Stern−Volmer plots between F_0/F and $[Pd^{2+}]$ was employed to determine its K_{sv} value. Consequently, the K_{sv} value obtained upon the gradual addition of Pd^{2+} was determined to be 1.6×10^4 M^{-1} indicating high levels of quenching, thus higher levels of sensitivity and binding interactions toward AUBM-6-NS. The obtained K_{sv} value is found to be comparable to other suspension-based Pd^{2+} sensors as shown in Table 2.

The sensitivity of AUBM-6-NS toward Pd^{2+} is demonstrated to be among the lowest detected, by which its detection limit was found to be 0.02 ppm, which is much beneath the permissible limit set by World Health Organization (WHO) for Pd^{2+} in drug chemicals (5−10 ppm).[7] Moreover, since the Stern−Volmer plot represents a straight line, the presence of dynamic (collisional) quenching is concluded to deactivate the fluorescent excited state of AUBM-6-NS, thus decreasing its luminescent intensity. The proposed mechanism of such quenching relies behind the π-philic nature of Pd^{2+}, which may coordinate with the unsaturated alkene moieties (−CH═CH−) present in INA ligand through π−d transitions (Figure S14).[9] Moreover, according to the Pearson acid−base (HSAB) concept, the pyridine functional group in INA ligand, being a borderline base (electron pair donor), may act to enhance the electron transfer to Pd^{2+} ions that are known to be soft acids (electron pair acceptors),[42] which in return may explain its high quenching selectivity. The stability of AUBM-6-NS was also studied, by which PXRD pattern of MOF crystals after sensing Pd^{2+} (Figure S2) was shown to be in agreement with that of the original sample, thus inferring the framework's stability after sensing.

Table 2. Literature Survey about Previously Reported Chemosensors towards Pd^{2+} Sensing[a]

chemo-sensor	selectivity	sensing method	LOD_{min} (ppb)	K_{sv} value (M^{-1})	ref
Zn-MOF	Fe^{3+} and Pd^{2+}	turn-off	35	4.2×10^4	40
Cd-MOF	Fe^{3+} and Pd^{2+}	turn-off	18	7.9×10^4	40
Zn-MOF	Pd^{2+} and PA	turn-off	30	3.6×10^4	9
Eu-MOF	Pd^{2+}	turn-off	44	7.8×10^4	41
RPd4	Pd^{2+}	turn-on	50	NA	10
AUBM-6-NS	Pd^{2+}	turn-off	20	1.6×10^4	this work

[a]PA: picric acid. NA: not applicable.

CONCLUSIONS

A metal organic framework (AUBM-6) structure is successfully synthesized and fully characterized. The synthesized MOF exhibits a 2D-layered topology that is activated into its luminescence sensing properties via top-down liquid ultrasonication exfoliation of its bulk topology into a few-layer nanosheets. PL investigations of AUBM-6-NS exhibit a ratiometric response toward acetone and a selective and highly sensitive turn-off quenching mechanism toward Pd^{2+} at trace concentrations, even in the presence of competing metal ions. The mutual existence of a ratiometic and turn-off probe suggests the presence of energy and electron transfer mechanisms, which amplified AUBM-6-NS selectivity toward acetone and Pd^{2+}, respectively. The detection of Pd^{2+} was among the lowest reported, which is also below the permissible limits set by WHO. Moreover, the present work may be of great potential, demonstrating a dual-sensing fluorescent MOF as acetone sensor for medical diagnostics and monitoring, as well as Pd^{2+} ion detection present in reaction vessels, thus preventing hazardous environmental and health concerns.

ASSOCIATED CONTENT

Supporting Information

The Supporting Information is available free of charge on the ACS Publications website at DOI: 10.1021/acs.inorgchem.9b01315.

Crystallographic data in CIF format, crystallographic refinement data, additional structure images, SEM, PXRD, TGA, FT-IR, and UV−visible absorption spectra, additional titration experiments at different pH, competition titration experiments, proposed scheme for quenching mechanism of Pd^{2+} (PDF)

Accession Codes

CCDC 1904768 contains the supplementary crystallographic data for this paper. These data can be obtained free of charge via www.ccdc.cam.ac.uk/data_request/cif, or by emailing data_request@ccdc.cam.ac.uk, or by contacting The Cam-

DOI: 10.1021/acs.inorgchem.9b01315
Inorg. Chem. 2019, 58, 10912−10919

bridge Crystallographic Data Centre, 12 Union Road, Cambridge CB2 1EZ, UK; fax: +44 1223 336033.

AUTHOR INFORMATION

Corresponding Author

*E-mail: mohamad.hmadeh@aub.edu.lb.

ORCID

Mohamad Hmadeh: 0000-0003-3027-3192

Notes

The authors declare no competing financial interest.

ACKNOWLEDGMENTS

The authors gratefully acknowledge the funding provided by the American University of Beirut Research Board and the K. Shair Central Research Science Laboratory. We also acknowledge the Lebanese National Council for Scientific Research Award Nos. A103496 and A103487. We are also grateful to S. Al Natour for the graphical illustrations demonstrated in this work.

REFERENCES

(1) Rowsell, J. L. C.; Yaghi, O. M. Metal-Organic Frameworks: A New Class of Porous Materials. *Microporous Mesoporous Mater.* **2004**, *73*, 3−14.

(2) Zhou, H. C. J.; Kitagawa, S. Metal-Organic Frameworks (MOFs). *Chem. Soc. Rev.* **2014**, *43* (16), 5415−5418.

(3) Rosi, N. L.; Eddaoudi, M.; Kim, J.; O'Keeffe, M.; Yaghi, O. M. Advances in the Chemistry of Metal - Organic Frameworks Paper Highlight. *CrystEngComm* **2002**, *4*, 401−404.

(4) Moghadam, P. Z.; Islamoglu, T.; Goswami, S.; Exley, J.; Fantham, M.; Kaminski, C. F.; Snurr, R. Q.; Farha, O. K.; Fairen-Jimenez, D. Computer-Aided Discovery of a Metal-Organic Framework with Superior Oxygen Uptake. *Nat. Commun.* **2018**, *9* (1), 1−8.

(5) Jrad, A.; Abu Tarboush, B. J.; Hmadeh, M.; Ahmad, M. Tuning Acidity in Zirconium-Based Metal Organic Frameworks Catalysts for Enhanced Production of Butyl Butyrate Applied Catalysis A, General Tuning Acidity in Zirconium-Based Metal Organic Frameworks Catalysts for Enhanced Production of Butyl Butyrate. *Appl. Catal., A* **2019**, *570*, 31−41.

(6) Atallah, H.; ELcheikh Mahmoud, M.; Jelle, A.; Lough, A.; Hmadeh, M. A Highly Stable Indium Based Metal Organic Framework for Efficient Arsenic Removal from Water. *Dalt. Trans.* **2018**, *47*, 3−14.

(7) Melber, C.; Keller, D.; Mangelsdorf, I. Palladium, Environmental Healthy Criteria Series 226; 2002. Online at https://apps.who.int/iris/handle/10665/42401.

(8) Kumar, P.; Kumar, V.; Gupta, R. Selective Fluorescent Turn-off Sensing of Pd2+ Ion: Applications as Paper Strips, Polystyrene Films, and in Cell Imaging. *RSC Adv.* **2017**, *7*, 7734−7741.

(9) Sanda, S.; Parshamoni, S.; Biswas, S.; Konar, S. Highly Selective Detection of Palladium and Picric Acid by a Luminescent MOF: A Dual Functional Fluorescent Sensor. *Chem. Commun.* **2015**, *51* (30), 6576−6579.

(10) Li, H.; Fan, J.; Hu, M.; Cheng, G.; Zhou, D.; et al. Highly Sensitive and Fast-Responsive Fluorescent Chemosensor for Palladium: Reversible Sensing and Visible Recovery. *Chem. - Eur. J.* **2012**, *18*, 12242−12250.

(11) Garrett, C. E.; Prasad, K. The Art of Meeting Palladium Specifications in Active Pharmaceutical Ingredients Produced by Pd-Catalyzed Reactions. *Adv. Synth. Catal.* **2004**, *346*, 889−900.

(12) Li, H.; Fan, J.; Du, J.; Guo, K.; Sun, S.; Liu, X.; Peng, X. A Fluorescent and Colorimetric Probe Specific for Palladium Detection W. *Chem. Commun.* **2010**, *46*, 1079−1081.

(13) Zhao, M.; Yao, Z. Q.; Xu, Y. L.; Chang, Z.; Bu, X. H. Guest Dependent Structure and Acetone Sensing Properties of a 2D Eu^{3+} coordination Polymer. *RSC Adv.* **2017**, *7* (4), 2258−2263.

(14) Allendorf, M. D.; Bauer, C. A.; Bhakta, R. K.; Houk, R. J. T. Luminescent Metal-Organic Frameworks. *Chem. Soc. Rev.* **2009**, *38* (5), 1330−1352.

(15) Cui, Y.; Zhang, J.; Chen, B.; Qian, G. Lanthanide Metal-Organic Frameworks for Luminescent Applications. *Elsevier* **2016**, *50*, 243−268.

(16) Li, Y. L.; Zhao, Y.; Wang, P.; Kang, Y. S.; Liu, Q.; Zhang, X. Du; Sun, W. Y. Multifunctional Metal-Organic Frameworks with Fluorescent Sensing and Selective Adsorption Properties. *Inorg. Chem.* **2016**, *55* (22), 11821−11830.

(17) Chen, B.; Yang, Y.; Zapata, F.; Lin, G.; Qian, G.; Lobkovsky, E. B. Luminescent Open Metal Sites within a Metal-Organic Framework for Sensing Small Molecules. *Adv. Mater.* **2007**, *19* (13), 1693−1696.

(18) Zhang, Q.; Wang, J.; Kirillov, A. M.; Dou, W.; et al. Multifunctional Ln-MOF Luminescent Probe for Efficient Sensing of Fe^{3+}, Ce^{3+} and Acetone. *ACS Appl. Mater. Interfaces* **2018**, *10*, 23976−23986.

(19) Zhang, X.; Su, F.; Chen, D.; Peng, Y.; Guo, W.; Liu, C.; Du, M. A Water-Stable EuIII-Based MOF as a Dual-Emission Luminescent Sensor for Discriminative Detection of Nitroaromatic Pollutants. *Dalt. Trans.* **2019**, *48*, 1843−1849.

(20) Cui, Y.; Xu, H.; Yue, Y.; Guo, Z.; Yu, J.; Chen, Z.; Gao, J.; Yang, Y.; Qian, G.; Chen, B. A Luminescent Mixed-Lanthanide Metal-Organic Framework Thermometer. *J. Am. Chem. Soc.* **2012**, *134* (9), 3979−3982.

(21) Cui, Y.; Yue, Y.; Qian, G.; Chen, B. Luminescent Functional Metal-Organic Frameworks. *Chem. Rev.* **2012**, *112* (2), 1126−1162.

(22) Hassan, G.; El Hoda Saad, N.; Hmadeh, M.; Karam, P. Enhancing Porphyrin Photostability When Locked in Metal-Organic Frameworks. *Dalton Trans.* **2018**, *47*, 15765−15771.

(23) Xiang, Z.; Fang, C.; Leng, S.; Cao, D. An Amino Group Functionalized Metal-Organic Framework as a Luminescent Probe for Highly Selective Sensing of Fe^{3+} Ions. *J. Mater. Chem. A* **2014**, *2* (21), 7662−7665.

(24) Xu, H.; Dong, Y.; Wu, Y.; Ren, W.; Zhao, T.; Wang, S.; Gao, J. An -OH Group Functionalized MOF for Ratiometric Fe^{3+} Sensing. *J. Solid State Chem.* **2018**, *258*, 441−446.

(25) Xu, H.; Gao, J.; Qian, X.; Wang, J.; He, H.; Cui, Y.; Yang, Y.; Wang, Z.; Qian, G. Metal-Organic Framework Nanosheets for Fast-Response and Highly Sensitive Luminescent Sensing of Fe^{3+}. *J. Mater. Chem. A* **2016**, *4* (28), 10900−10905.

(26) Lan, A.; Li, K.; Wu, H.; Olson, D. H.; Emge, T. J.; Ki, W.; Hong, M.; Li, J. A Luminescent Microporous Metal-Organic Framework for the Fast Andreversible Detection of High Explosives. *Angew. Chem., Int. Ed.* **2009**, *48* (13), 2334−2338.

(27) Fang, Q.; Zhu, G.; Xue, M.; Sun, J.; Sun, F.; Qiu, S. Structure, Luminescence, and Adsorption Properties of Two Chiral Microporous Metal-Organic Frameworks. *Inorg. Chem.* **2006**, *45* (9), 3582−3587.

(28) Pramanik, S.; Zheng, C.; Zhang, X.; Emge, T. J.; Li, J. New Microporous Metal-Organic Framework Demonstrating Unique Selectivity for Detection of High Explosives and Aromatic Compounds. *J. Am. Chem. Soc.* **2011**, *133* (12), 4153−4155.

(29) Naguib, M.; Gogotsi, Y. Synthesis of Two-Dimensional Materials by Selective Extraction. *Acc. Chem. Res.* **2015**, *48*, 128−135.

(30) Peng, Y.; Li, Y.; Ban, Y.; Jin, H.; Jiao, W.; Liu, X.; Yang, W. Metal- Organic Framework Nanosheets as Building Blocks for Molecular Sieving Membranes. *Science* **2014**, *346* (6215), 1356−1359.

(31) Ding, Y.; Chen, Y. P.; Zhang, X.; Chen, L.; Dong, Z.; Jiang, H. L.; Xu, H.; Zhou, H. C. Controlled Intercalation and Chemical Exfoliation of Layered Metal-Organic Frameworks Using a Chemically Labile Intercalating Agent. *J. Am. Chem. Soc.* **2017**, *139* (27), 9136−9139.

(32) Niu, L.; Coleman, J. N.; Zhang, H.; Shin, H.; Chhowalla, M.; Zheng, Z. Production of Two-Dimensional Nanomaterials via Liquid-Based Direct Exfoliation. *Small* **2016**, *12* (3), 272−293.

(33) Xiao, Y.; Cui, Y.; Zheng, Q.; Xiang, S.; Qian, G.; Chen, B. A Microporous Luminescent Metal-Organic Framework for Highly

DOI: 10.1021/acs.inorgchem.9b01315
Inorg. Chem. 2019, 58, 10912−10919

Selective and Sensitive Sensing of Cu^{2+} in Aqueous Solution. *Chem. Commun.* **2010**, *46* (30), 5503−5505.
(34) Yang, L.; Powell, D. R.; Houser, R. P. Structural Variation in Copper(I) Complexes with Pyridylmethylamide Ligands: Structural Analysis with a New Four-Coordinate Geometry Index. *Dalt. Trans.* **2007**, 955−964.
(35) Marlin, D. S.; Olmstead, M. M.; Mascharak, P. K. Structure - Spectroscopy Correlation in Distorted Five-Coordinate Cu (II) Complexes: A Case Study with a Set of Closely Related Copper Complexes of Pyridine-2,6-dicarboxamide Ligands. *Inorg. Chem.* **2001**, *40*, 7003−7008.
(36) Guo, Z.; Xu, H.; Su, S.; Cai, J.; Dang, S.; Xiang, S.; Qian, G.; Zhang, H.; O'keeffe, M.; Chen, B. A Robust near Infrared Luminescent Ytterbium Metal - Organic Framework for Sensing of Small Molecules W. *Chem. Commun.* **2011**, *47*, 5551−5553.
(37) Yang, W.; Feng, J.; Zhang, H. Facile and Rapid Fabrication of Nanostructured Lanthanide Coordination Polymers as Selective Luminescent Probes in Aqueous Solution. *J. Mater. Chem.* **2012**, *22*, 6819−6823.
(38) Yi, F.; Yang, W.; Sun, Z. Highly Selective Acetone Fluorescent Sensors Based on Microporous Cd(II) MetalOrganic Frameworks. *J. Mater. Chem.* **2012**, *22*, 23201−23209.
(39) van Middlesworth, J. M.; Wood, S. The Stability of Palladium(II) Hydroxide and Hydroxy Chloride Complexes: An Experimental Solubility Study at 25 - 85 °C and 1 bar. *Geochim. Cosmochim. Acta* **1999**, *63* (11), 1751−1765.
(40) Parmar, B.; Rachuri, Y.; Bisht, K. K.; Suresh, E. Mixed-Ligand LMOF Fluorosensors for Detection of Cr(VI) Oxyanions and Fe^{3+} /Pd^{2+} Cations in Aqueous Media. *Inorg. Chem.* **2017**, *56* (Vi), 10939−10949.
(41) Helal, A.; Nguyen, H. L.; Al-Ahmed, A.; Cordova, K. E.; Yamani, Z. H. An Ultrasensitive and Selective Metal-Organic Framework Chemosensor for Palladium Detection in Water. *Inorg. Chem.* **2019**, *58*, 1738−1741.
(42) Balamurugan, R.; Liu, J.; Liu, B. A Review of RecentDevelopments in Fluorescent Sensors for the SelectiveDetection of Palladium Ions. *Coord. Chem. Rev.* **2018**, *376*, 196−224.

DOI: 10.1021/acs.inorgchem.9b01315
Inorg. Chem. 2019, 58, 10912−10919